Cellulose Nanocrystals Reinforced Shape Memory Polymer Cardiovascular Stent

1 Introduction

Stents are vascular implants that are used to open passageways of anatomical vessels. In recent years, challenges in cardiovascular implants are mostly encountered in the area of customized stents. The treatment of coronary bifurcation lesions is one example (Foin et al., 2013). Additive manufacturing can be the best option for personalized stents (Finazzi et al., 2019). Several works have discussed the application of additive manufacturing in fabricating metallic cardiovascular stents (Finazzi et al., 2019; Wen et al., 2018). However, one major limitation for metallic stents is that the majority of them are not self-deployable, which means that an invasive surgery is still needed.

Shape memory materials (SMMs) can be an alternative material for cardiovascular stents to achieve self-deployment (Huang et al., 2011). SMMs are smart materials that can be programmed to maintain a temporary shape until a proper stimulus is applied. After the stimulation, the original shape will be recovered. Wache et al. developed the first thermo-responsive shape memory polymer (SMP) stents by injection-molding (Wache et al., 2003). Although the ability of self-expansion was demonstrated, the geometry of the stents, which was a circular tube with solid walls, could not be used as meshes are required in the stent design (Finazzi et al., 2019). Later, different SMPs were used to fabricate cardiovascular stents. Among them, polyurethane(PU)-based SMPs attracted much attention due to its biocompatibility, recyclability and tailorability (Huang et al., 2011).

To produce customized stents from thermoplastic SMP, the extrusion-based-additive-manufacturing (EBAM) technique is an ideal method due to its tailorability, low-cost and availability. EBAM melts thermoplastic polymers and builds customized 3D objects layer-by-layer using extrusion. Only (Jia et al., 2018) and (Cabrera et al., 2017) fabricated thermoplastic SMP stents using EBAM. However, in Jia et al., the recovery of their stents was conducted under 70°C, which is too high to be used in human body (Jia et al., 2018). In Cabrera et al., although the stent was able to recover at 37°C, the maximum force that their stents could support decayed to nearly 0 N after twenty days (Cabrera et al., 2017). Fortunately, these limitations can be overcome by fabricating SMP with reinforcements (Zhao et al., 2019).

Cellulose nanocrystals (CNCs) are rod-like nanoparticles with high elastic moduli (100-140 GPa) and high aspect ratio (diameter of 5-20 nm and length of hundreds of nanometers) (Klemm et al., 2005). They are promising reinforcements for stent applications as they can enhance the mechanical properties with relatively low concentration (a few wt%) (Han, Lu, Yue, et al., 2019; Han, Wang, Yue, et al., 2019; Han, Wang, Zhu, et al., 2019). Also, cellulose is bio-friendly and bio-compatible, which poses less health and environmental concerns (Ding et al., 2018; Han, Ding, Mei, et al., 2019; Klemm et al., 2005) compared to other nanoparticles, such as carbon nanotubes. In terms of polymer compatibility, CNCs possess abundant hydroxyl groups on the surface, which could potentially form hydrogen bonding on the interface during the fabrication of PU/CNC composites (Chakrabarty and Teramoto, 2018). Based on these facts, PU and CNCs can be identified as compatible candidates for the fabrication of polymer composites (Özgür

Seydibeyoğlu and Oksman, 2008). In our group's previous work, CNCs have been successfully embedded into PU-based SMP matrix with simple melt-mixing technique, and they were shown to improve the toughness, flexural modulus and recovery properties of the nanocomposites (Garces et al., 2018).

The objective of this study is to report an innovative method to fabricate customizable and tailorable CNC reinforced PU-based SMP stents using EBAM. Firstly, we produced and characterized the CNC reinforced PU filaments. Then, the stents were fabricated by an EBAM system, programmed to a compact temporary shape, and activated to recover their original shape. The recovery properties of the stents, such as recovery ratio and recovery force with respect to time were characterized. The results indicated that the fabricated and programmed stents provided sufficient recovery force compared to commercially available stents. At this initial portion of the overall work, only straight stents were fabricated and investigated, but this fabrication method can be easily extended to other shapes (e.g. bifurcated stents).

2 Experimental methodology

2.1 Materials

PU-based SMP pellets with a glass transition temperature (T_g) prescribed as 45°C (MM4520) was purchased from SMP Technologies (Japan). According to the manufacturer provided technical data sheet, MM4520 has a specific gravity of 1.25 and was prepared from diphenylmethane-4,4'-diisocyanate, adipic acid, ethylene glycol, ethylene oxide, polypropylene oxide, 1,4-butanediol and bisphenol A. The CNC particles were supplied by InnoTech Alberta (Edmonton, Canada), with aspect ratio (length to diameter) of 11.9±3.1. All materials were used as received without further purification.

2.2 Melt-compounding and filament production

There were two extrusion steps involved in the filament production. The first was melt-compounding extrusion. SMP pellets and CNC powders were vacuum dried at a constant temperature of 100°C for 24h in a Lindberg/Blue M™ vacuum oven (Thermo Fisher Scientific, USA). After the drying, the materials were physically mixed in solid state with CNC loadings of 0, 1, 4, 7 wt% in the composites. PRISM USALAB 16 twin-screw extruder (Thermo Fisher Scientific, USA) was used to perform the melt-compounding extrusion. Based on our group's previous works (Garces et al., 2018; Villacres et al., 2018), the nozzle temperature was set at 230°C and there was a 5°C decrement in each of the three subsequent heating zones towards the hopper. After the extrusion, the materials were cooled in a water bath and pelletized with a length of 1mm.

The second step was filament production. The composite pellets were again dried in Lindberg/Blue M™ vacuum oven at a constant temperature of 100°C for 24h. Brabender™ single screw extruder (C.W. Brabender Instruments, Inc., Germany) was then used for filament production, with the same parameters setting as in melt-compounding extrusion. Filaments with diameter of 2.80±0.5 mm were produced and wound onto a standard-sized desktop 3D printing spool.

2.3 Stent fabrication

The stent with a length of 15 mm, an inner diameter of 3 mm and an outer diameter of 4.6 mm was designed in a braid-like geometry, as shown in Figure 1. The digital model of the stent was built using a CAD/CAM software and Ultimaker Cura™ (Ultimaker B.V., Netherlands) was used to generate the G-code. After that, the CNC/SMP composite filaments with different CNC

loadings were fed into an EBAM type printer, Ultimaker 3™ (Ultimaker B.V., Netherlands), with a nozzle diameter of 0.4 mm. The key printing parameters are shown in Table 1.

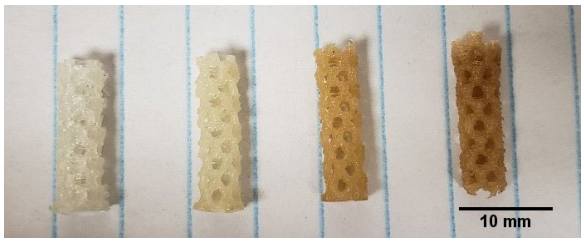

Figure 1. CNC-reinforced SMP cardiovascular stents fabricated by EBAM, left to right: 0 wt%, 1 wt%, 4 wt% and 7 wt% of CNC reinforcement.

Table 1. Key printing parameters for the stents with different CNC loadings

2.4 Shape memory effect (SME) programing

All stent samples were dried in Lindberg/Blue M™ vacuum oven (Thermo Fisher Scientific, USA) at 100°C overnight (approximately 15h) to avoid the effect of moisture. The programming was conducted on ElectroForce 3200 Series III (Bose Corporation, USA) equipped with a 450N load cell and two compression plates, as shown in Figure 2. The programming started with compressing the stent radially at 45±0.2°C for a displacement of 2 mm. After that, the compression displacement was maintained, and the stents were cooled to room temperature (23±1°C). For pure SMP stents, the force on the compression plate reduced to 0 N when the sample was cooled down completely. However, for CNC reinforced samples, there was a residual force due to the lack of SME of the CNCs. In those cases, the upper compression plate was retracted until the residual force reached 0 N.

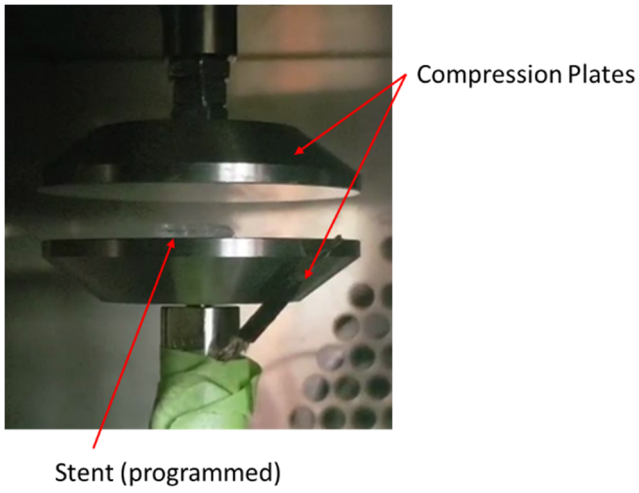

Figure 2. Machine configuration during the programming.

2.5 Characterizations

2.5.1 Modulated differential scanning calorimetry (modulated DSC)

Modulated DSC on filament samples was conducted with DSC Q100 (TA instruments, USA) to measure the transition temperatures. The modulation was ±1.00°C every 60 s. The heating rate was 5°C/min and the heating range was -20 to 250°C. Prior to the characterizations, all samples were heated to 150°C, then cooled down to -20°C in order to erase the thermal history induced by the extrusion processes.

2.5.2 Thermo-gravimetric analysis (TGA)

Thermo-gravimetric analysis on stent samples with different CNC loadings was conducted using TGA Q50 (TA instruments, USA) to quantify their thermal stability (i.e., degradation temperatures). A heating rate of 10°C/min was used and the temperature range was 25-600°C. The analysis was operated in air.

2.5.3 Recovery force characterizations

In the recovery force characterization, the programmed samples were reheated to 40±0.2°C immediately after the programming process. Since the displacement of the compression plates was maintained, the force exerted on the compression plates was recorded for 30 min after the start of the reheating process. This force was further divided by the length of the stents (15 mm) to obtain the recovery force (in N/mm) reported in this work.

2.5.4 Recovery ratio characterizations

To characterize the recovery ratio, the programmed stents were taken from the universal tensile testing system and placed in Lindberg/Blue M™ radiation oven (Thermo Fisher Scientific, Waltham, USA) at a temperature of 40±0.1°C. A photonics measurement system consists of a Basler acA3800-10gm camera (Basler, USA) and DL097 light source (Advanced Illumination, USA) was used to record the shape of the stents within 30 min after the application of 40°C temperature. A graphical illustration of the geometry of a stent before programming, after programing and during recovery is shown in Figure 3, where the height of the stent as a function of time, $h(t)$, was recorded every 5 min and analyzed by a Java code implemented on ImageJ. Because there were slight variations in the dimensions of the samples, a normalized recovery ratio ξ based on the following definition was used (Hu, 2007):

$$\xi = \frac{h(t) - h_0}{H - h_0} \tag{1}$$

where H and h_0 are respectively the heights of the stent before and after programming (see Figure 3).

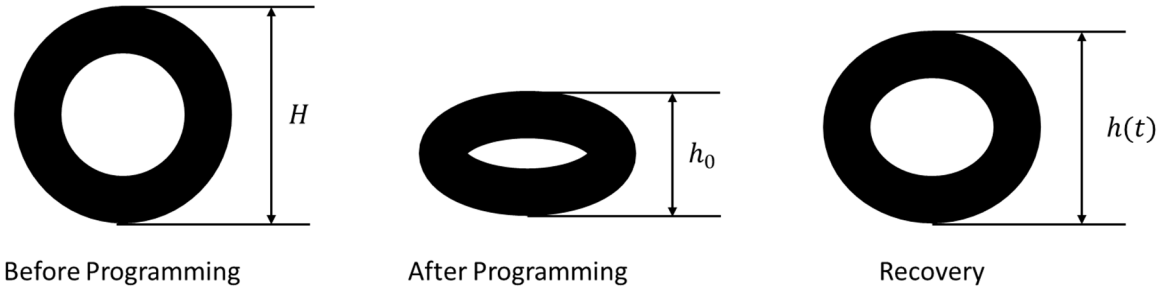

Figure 3. Graphical illustration of the stent programming and recovery process, as well as the dimensions that were measured to quantify the recovery ratio.

3 Results and discussion

3.1 Thermal characterizations

3.1.1 Modulated DSC

The modulated DSC were conducted to obtain the glass transition (T_g) and melting (T_m) temperatures of the polymer composites. The change of heat flow with respect to temperature is shown in Figure 4 (a) and the measured T_g and T_m are shown in Table 2. The addition of up to 7 wt% CNC did not change T_m significantly. Similar results were also obtained in previous work (Garces et al., 2018). Although the start of melting was seen at around 156°C in the DSC results, this temperature could not be used as the printing temperature in the EBAM process. The printing temperature for the filaments needed to be higher in order for the molten material to have an appropriate viscosity to flow through the nozzle (Mohamed et al., 2015). Based on our group's previous work (Villacres et al., 2018), the printing temperature was set at 210°C and 215°C (Table 1) to ensure adequate melting and flowing of the filaments.

The unreinforced SMP showed a T_g of 39.7°C, which was slightly lower than the prescribed value (45°C). The difference might be caused by the difference in the selection of characterizing parameters during the modulated DSC (Huang et al., 2011). From Table 2 there was a slight drop of around 5°C in T_g when CNCs were added at 1 wt%. As the amount of CNC further increases, T_g remained stable. Similar results were also reported earlier (Garces et al., 2018). The reduction of T_g implies that the CNC addition may enhance the recovery performance of the material, since the recovery of an SMP was typically triggered at around T_g (Huang et al., 2011). As a result, the stents were expected to acquire a higher recovery force and better recovery ratio under the same activation temperature (40°C).

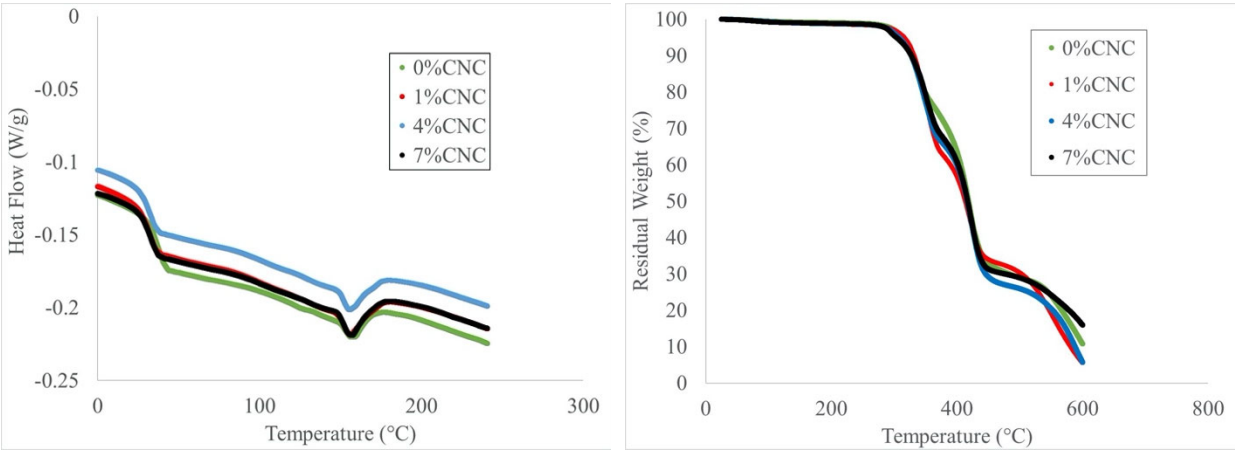

(a) (b)

Figure 4. Thermal characterization (a) modulated DSC of the filaments, and (b) TGA of the printed samples.

Table 2. Measured T_g and T_m from modulated DSC characterizations

3.1.2 TGA

TGA of the printed stent samples were performed to obtain the expected degradation temperatures and the results are shown in Figure 4 (b). Pure SMP sample (0% CNC) and the CNC loaded samples all displayed similar multi-step degradation. Significant degradation did not occur until 280°C, indicating that the stents were stable below 280°C. The TGA result of pure CNC, not presented here as it is part of another publication in preparation, showed no severe degradation until 240°C. The printing temperature was below 220°C, which was lower than the CNC degradation temperatures measured from TGA, ensuring the integrity of the materials. However, as shown in Figure 1, the color of the stents became darker as the CNC loading increases. This implies that the surface of the CNCs might have experienced some minor thermal degradation during the extrusion processes or printing.

3.2 Recovery characterizations

3.2.1 Recovery force

As mentioned in section 2.4, there was a residual force due to the lack of SME of the CNCs. The average residual force is shown in Table 3 which increases with the CNC loadings. Huang et al. proposed the shape memory mechanism for PU-based SMP by assuming elastic and transition segments, as shown in Figure 5(a) (Huang et al., 2011). Transition segments will be softened when heated above T_g, and hardened when cooled down below T_g. As a result, after cooling, SMP can maintain a temporary shape without the exertion of an external force. Wu et al. demonstrated that CNCs behaved like a linear elastic material at room temperature (Wu et al., 2010). Szcześniak et al. determined T_g of dry cellulose to be in the range of 200 to 240°C (Szcześniak et al., 2008). Therefore, under our experimental condition (temperature range 23-40°C), CNCs were expected to behave like a linear elastic material. In addition, CNCs were found to have a high Young's modulus of 100-140GPa (Garces et al., 2018; Klemm et al., 2005; Nicharat et al., 2017). By adding CNCs, the elastic component effectively increased (see Figure 5 (b)), leading to the appearance of a residual force after cooling. After retracting the upper compression plate for a certain displacement, a new balance between the elastic component (elastic segment in SMP and CNC) and the transition segment was achieved, and the residual force reduced to zero. The average retraction displacement is also shown in Table 3, which as expected increased with the CNC loadings.

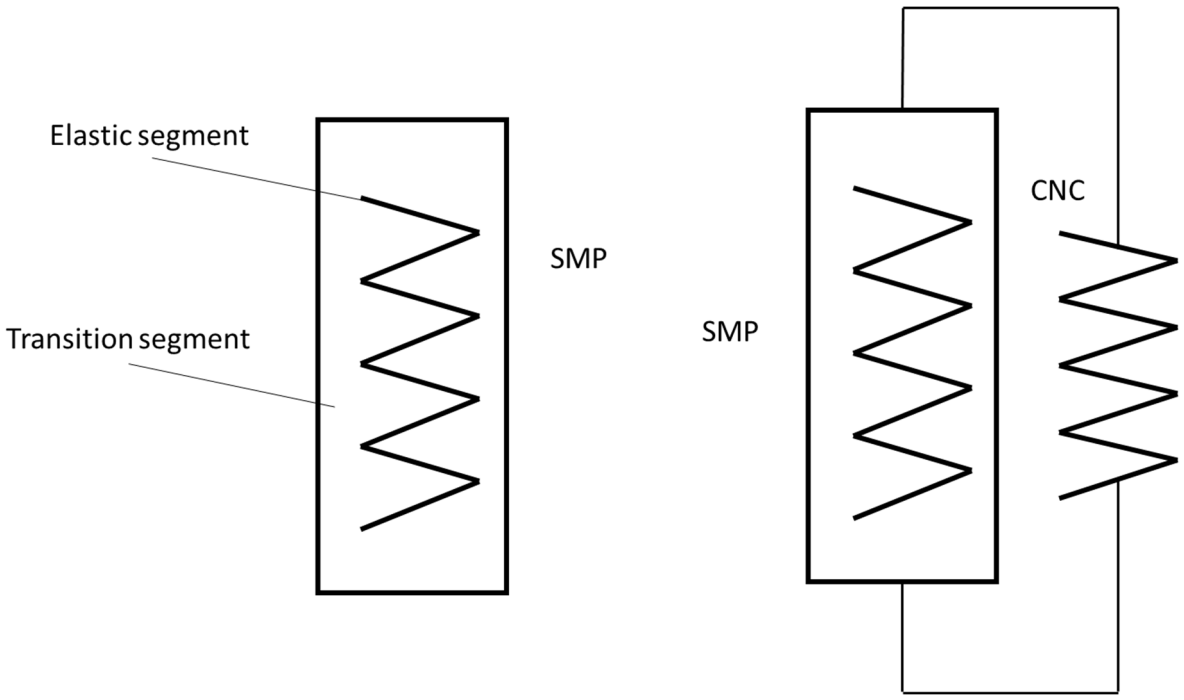

Figure 5. an illustration of the shape memory mechanism of (a) pure SMP and (b) CNC reinforced SMP composites

Table 3. Summary of the average residual force and average retraction displacement to remove the residual force

Figure 6 shows the time-evolution of the recovery forces (normalized by the length of the stent, in N/mm) for different CNC loadings. Three different colors in each subfigure correspond to the three identically printed and programmed stent samples. There were slight variations in the recovery force between the three samples, which is most likely due to the braided shape, and hence the anisotropic nature, of the stents. Although the outer contour of the stents was designed to be circular, the actual shape was not entirely circular or symmetric. There were many different ways of placing the stent between the compression plates, and Figure 7 shows two examples. Difference in placements, which could not be precisely controlled in our experiments, could affect the way in which the stent was compressed which in turn caused the variations in the recovery force seen in Figure 6.

In Figure 6 (a), without CNC loadings, the recovery force reached a peak value after 4 min of activation and then quickly lowered down to a steady-state value. The decrease in the recovery force after the peak was caused by stress relaxation of the SMP. The peak recovery force was less than 0.2 N/mm in all three samples and the steady-state force after relaxation was around 0.05 N/mm. However, as can be seen from Figure 6 (b), (c) and (d), the recovery force increased to a plateau value after 10 min of activation and remained stable afterwards. The addition of a small amount of CNC was able to remove stress relaxation by acting as a stiff elastic component (see Figure 5(b)) at the activation temperature of 40°C. One representative curve was extracted from each sub-figure in Figure 6 and they are plotted together in Figure 8 for a quantitative comparison.

As expected, the steady-state recovery force increased with the CNC loading, from 0.05 N/mm at 0 wt% to around 0.4 N/mm at 7 wt%.

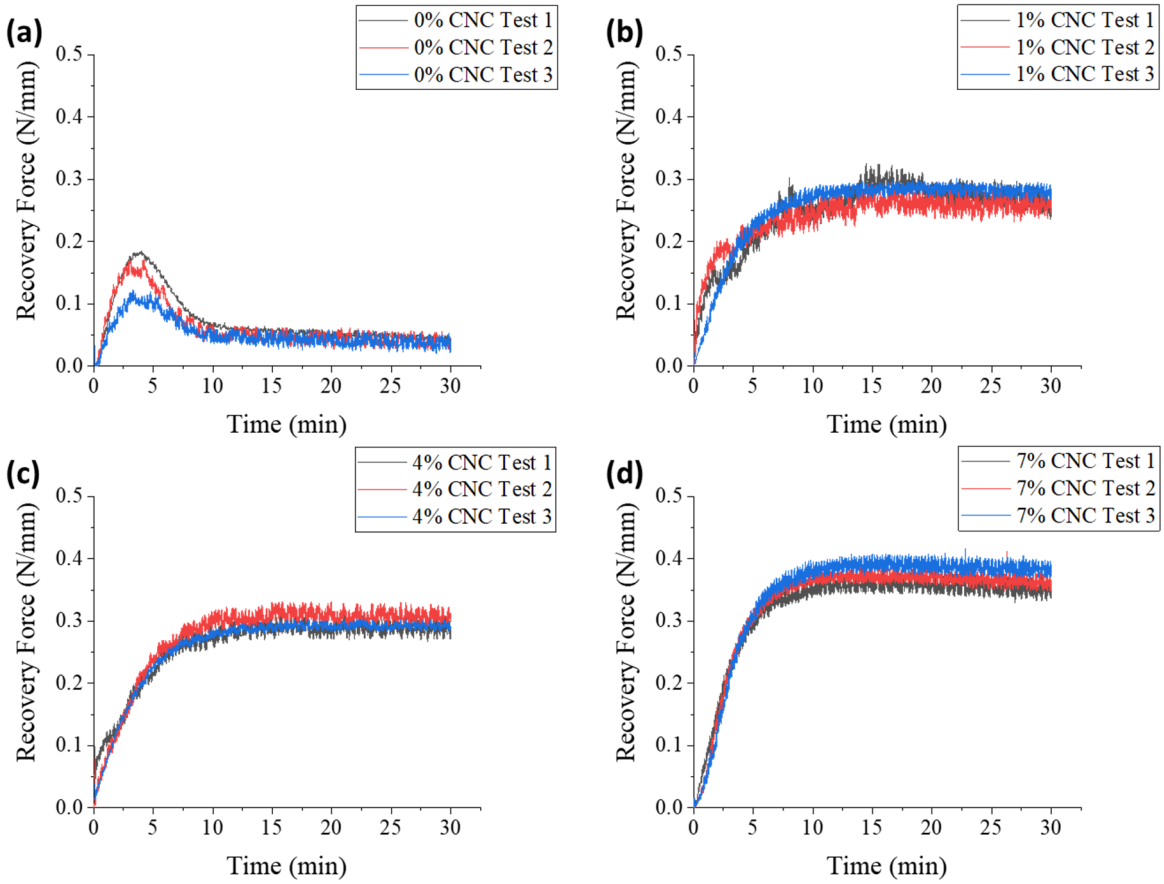

Figure 6. Recovery force of stents programmed at 45±0.2°C and recovered at 40±0.2°C. (a) 0 wt% CNC, (b) 1 wt% CNC, (c) 4 wt% CNC, (d) 7 wt% CNC. Each subfigure contains 3 curves corresponding to three identical but independent tests.

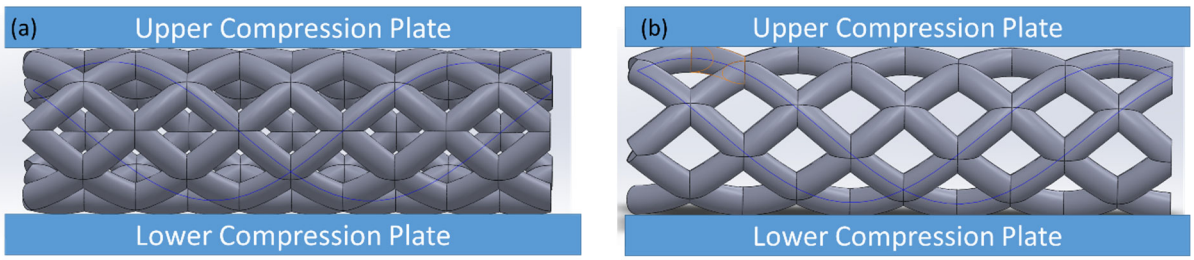

Figure 7. CAD model of stent braided structure showing two different ways of placing the stents between the compression plates.

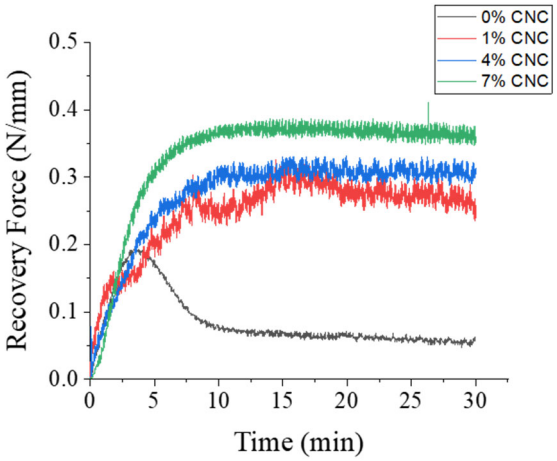

Figure 8. Representative recovery force curves of stents with different CNC loadings; all stents were programmed at 45±0.2°C and recovered at 40±0.2°C.

3.2.2 Recovery ratio

Figure 9 shows the recovery ratio calculated by equation (1). As mentioned in section 2.5.4, the recovery ratios of three samples at each CNC loadings were measured vs. time at 5 min intervals. The error bars in Figure 9 showed the standard deviations from the measurements of three samples. Since the prescribed T_g for MM4520 was 45°C, it was expected that under the activation temperature of 40°C, the pure SMP stent samples would barely recover (1.9±12.6% after 30 min). For CNC loadings between 0 wt% and 4 wt%, the recovery ratio after 30 min increased with increasing CNC loading, being 25.8±4.9% for 1 wt% CNC and 35.8±5.1% for 4 wt% CNC. The enhancement in recovery by adding CNC could be attributed to two effects. First, as mentioned in section 3.1.1, the addition of CNCs slightly reduced T_g of the materials. While this can partially explain the increase of recovery ratio from 0 wt% to 1 wt% CNC loadings, it cannot explain the increase from 1 wt% to 4 wt% as there was no apparent difference in T_g between them. The second reason is that with the increase of CNC loadings, the elastic components of the material increased (see Figure 5(b)), which also helped the recovery of the material.

On the contrary, at 7 wt% of CNCs, the final recovery ratio dropped to 27.6±14.5%. Also, the standard deviations were significantly large, as can be seen in Figure 9. The large variation and the decrease in average recovery ratio were suspected to be due to the agglomeration of CNCs, which was previously observed in our groups (Garces et al., 2018).

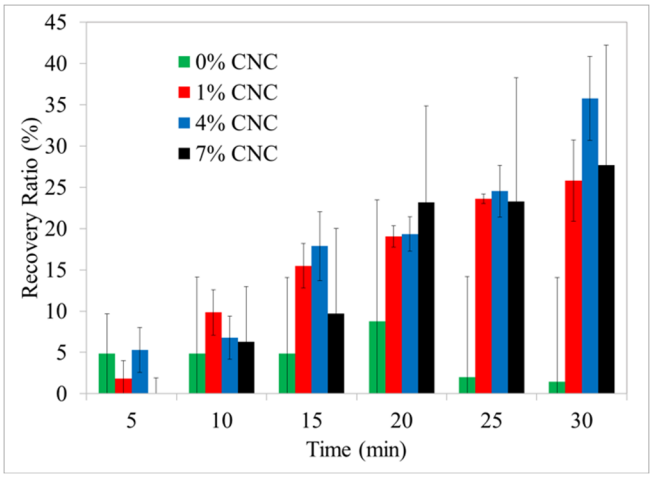

Figure 9. Calculated recovery ratio of the stents that recover at 40±0.1°C

3.3 Discussion

Table 2 shows that there was a reduction in T_g when CNCs were added. Along with the increased elastic response, better recovery performance was obtained under the same activation temperature of 40°C. This is an important advantage for the application of stents. Based on Dewhirst et al., the maximum time for which human cells sustained heating without severe damage increased by two order of magnitude when the exposure temperature dropped from 45°C to 40°C (Dewhirst et al., 2003). Lower activation temperature can significantly reduce tissue damage during the operation.

Krischek et al. compared the performance of 5 commercially available self-expandable stents. At 50% of radial compression, the largest recovery force was found on Wingspan (Boston Scientific), which was 0.0116 N/mm (Krischek et al., 2011). In the present study, the compression displacement was 2 mm and the outer diameter of the stents was 4.6 mm, so the radial compression was close to 50% as in Krischek et al. As can be seen from Figure 6 (a), even without the addition of CNC, the recovery force was one order of magnitude larger than Wingspan. The recovery force for 7% CNC reinforced stents was around 30 times larger than Wingspan. In addition, the stress relaxation of the stents during recovery was eliminated. This is another advantage in stent application because, for a self-deployable stent, a stable and large recovery force is required during the operation.

One major limitation for the as-prepared stent was that the final recovery ratio was too low for direct application. The recovery ratio only reached 35±5.1% when 4 wt% CNCs were added and this was the maximum recovery ratio obtained during the experiment. Several strategies can be used to reduce or remove this limitation. First of all, all the characterizations in this work were conducted in air and the stents were thoroughly dried in the vacuum oven. However, based on our group's previous work (Garces et al., 2019), T_g of SMP decreased significantly when moisture was absorbed into the matrix. It is therefore expected that the recovery ratio can increase significantly if the measurements are conducted in aqueous environment, which is similar to the end-use condition of the stents. Another strategy is to increase the activation temperature. Although as mentioned, exposure to higher temperature increased the probability of tissue damage, it has been shown by Dewhirst et al. that exposure to 45°C within 8 min was still safe for human cells (Dewhirst et al., 2003). Preliminary recovery ratio tests were performed for two identical PU-based

SMP stents without any CNC. As shown in Figure 10, when programmed at 45±0.2°C and recovered at 45±0.1°C, both of them were able to fully recover within 4 min.

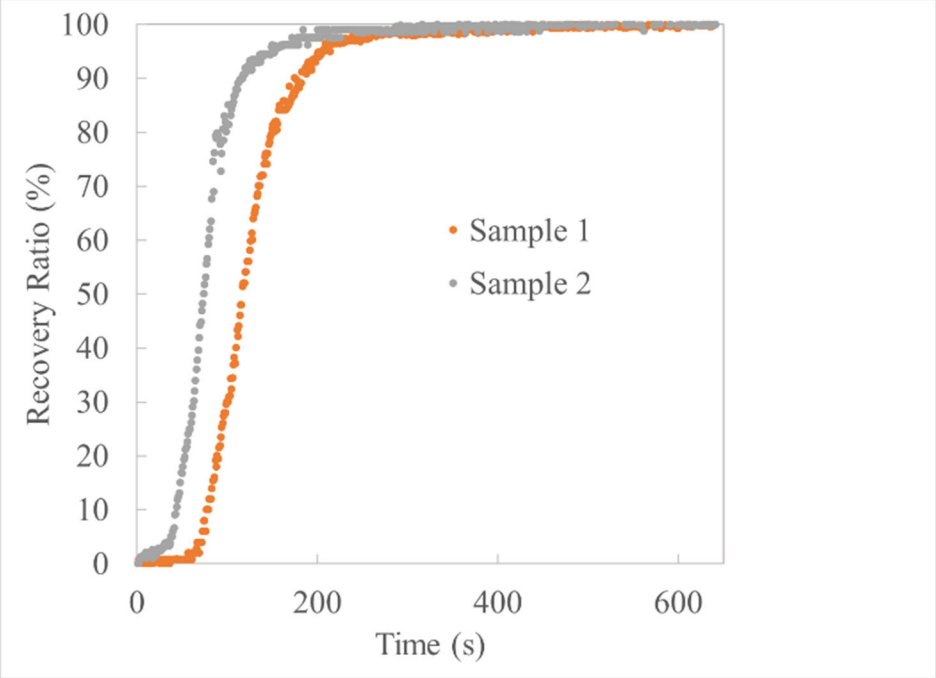

Figure 10. The time-dependent recovery ratio of two identical pure SMP stents programmed at 45±0.2°C and recovered at 45±0.1°C

4 Conclusion

This study proposed an innovative, fast and low-cost method to fabricate customized CNC reinforced PU based SMP composite stents using a commercial desktop EBAM system. Four different CNC loadings, 0, 1, 4 and 7 wt%, were added into SMP matrix to fabricate the composite stents. Thermo-characterizations, including TGA and modulated DSC were conducted on the as-prepared samples. TGA results indicated that the materials were stable during the fabrication process while modulated DSC results indicated that, with the addition of CNCs, the glass transition temperature dropped for about 5°C. The addition CNCs were able to reduce the T_g without affecting the thermal stability of the materials. The as-prepared stents were mechanically programmed at 45°C, and recovery force and recovery ratio measurements were conducted at 40°C. The results showed that the steady-state recovery force increased with the CNC loadings while the maximum recovery ratio was obtained at 4 wt% of CNCs. In comparison with commercially available stents, the fabricated and programmed stents provided sufficient recovery force required in the stenosed blood vessel. Consequently, these stents are good alternatives to the existing stents for treating coronary bifurcation lesions while offering tailorability, low cost, and speed of manufacturing.

5 References

Cabrera, M.S., Sanders, B., Goor, O.J.G.M., Driessen-Mol, A., Oomens, C.W.J. and Baaijens, F.P.T. (2017), "Computationally Designed 3D Printed Self-Expandable Polymer Stents with Biodegradation Capacity for Minimally Invasive Heart Valve Implantation: A Proof-of-Concept Study", *3D Printing and Additive Manufacturing*, Vol. 4 No. 1, pp. 19–29.

Chakrabarty, A. and Teramoto, Y. (2018), "Recent advances in nanocellulose composites with polymers: A guide for choosing partners and how to incorporate them", *Polymers*, Vol. 10 No. 5, pp. 517–564.

Dewhirst, M.W., Viglianti, B.L., Lora-michiels, M. and Hanson, M. (2003), "Thermal Dose Requirement for Tissue Effect: Experimental and Clinical Findings", *Proceedings - Society of Photo-Optical Instrumentation Engineers*, Vol. June 2 No. 4954, pp. 37–72.

Ding, Q., Xu, X., Yue, Y., Mei, C., Huang, C., Jiang, S., Wu, Q., et al. (2018), "Nanocellulose-Mediated Electroconductive Self-Healing Hydrogels with High Strength, Plasticity, Viscoelasticity, Stretchability, and Biocompatibility toward Multifunctional Applications", *ACS Applied Materials and Interfaces*, Vol. 10 No. 33, pp. 27987–28002.

Finazzi, V., Demir, A.G., Biffi, C.A., Chiastra, C., Migliavacca, F., Petrini, L. and Previtali, B. (2019), "Design Rules for Producing Cardiovascular Stents by Selective Laser Melting: Geometrical Constraints and Opportunities", *Procedia Structural Integrity*, Vol. 15, pp. 16–23.

Foin, N., Heart, N., Mattesini, A., Ospedaliero, A., Careggi, U. and Sen, S. (2013), "Tools & Techniques Clinical: Optimising stenting strategy in bifurcation lesions with insights from in vitro bifurcation models", *EuroIntervention*, Vol. 9 No. 7, pp. 885–887.

Garces, I.T., Aslanzadeh, S., Boluk, Y. and Ayranci, C. (2018), "Cellulose nanocrystals (CNC) reinforced shape memory polyurethane ribbons for future biomedical applications and design", *Journal of Thermoplastic Composite Materials*, Vol. 33 No. 3, pp. 377–392.

Garces, I.T., Aslanzadeh, S., Boluk, Y. and Ayranci, C. (2019), "Effect of moisture on shape memory polyurethane polymers for extrusion-based additive manufacturing", *Materials*, Vol. 12 No. 2, pp. 244–263.

Han, J., Ding, Q., Mei, C., Wu, Q., Yue, Y. and Xu, X. (2019), "An intrinsically self-healing and biocompatible electroconductive hydrogel based on nanostructured nanocellulose-polyaniline complexes embedded in a viscoelastic polymer network towards flexible conductors and electrodes", *Electrochimica Acta*, Vol. 318, pp. 660–672.

Han, J., Lu, K., Yue, Y., Mei, C., Huang, C., Wu, Q. and Xu, X. (2019), "Nanocellulose-templated assembly of polyaniline in natural rubber-based hybrid elastomers toward flexible electronic conductors", *Industrial Crops and Products*, Vol. 128, pp. 94–107.

Han, J., Wang, H., Yue, Y., Mei, C., Chen, J., Huang, C., Wu, Q., et al. (2019), "A self-healable and highly flexible supercapacitor integrated by dynamically cross-linked electro-conductive hydrogels based on nanocellulose-templated carbon nanotubes embedded in a viscoelastic polymer network", *Carbon*, Vol. 149, pp. 1–18.

Han, J., Wang, S., Zhu, S., Huang, C., Yue, Y., Mei, C., Xu, X., et al. (2019), "Electrospun Core-

Shell Nanofibrous Membranes with Nanocellulose-Stabilized Carbon Nanotubes for Use as High-Performance Flexible Supercapacitor Electrodes with Enhanced Water Resistance, Thermal Stability, and Mechanical Toughness", *ACS Applied Materials and Interfaces*, Vol. 11 No. 47, pp. 44624–44635.

Hu, J. (2007), *Shape Memory Polymers and Textiles*, 1st ed., Woodhead Publishing Limited, Cambridge, England.

Huang, W.M., Yap, B. and Fu, Y.Q. (2011), *Polyurethane Shape Memory Polymers*, 1st ed., CRC Press, Boca Raton, USA.

Jia, H., Gu, S.Y. and Chang, K. (2018), "3D printed self-expandable vascular stents from biodegradable shape memory polymer", *Advances in Polymer Technology*, Vol. 37 No. 8, pp. 3222–3228.

Klemm, D., Heublein, B., Fink, H.P. and Bohn, A. (2005), "Cellulose: Fascinating biopolymer and sustainable raw material", *Angewandte Chemie - International Edition*, Vol. 44 No. 22, pp. 3358–3393.

Krischek, Ö., Miloslavski, E., Fischer, S., Shrivastava, S. and Henkes, H. (2011), "A comparison of functional and physical properties of self-expanding intracranial stents [Neuroform3, Wingspan, Solitaire, Leo(+), Enterprise]", *Minimally Invasive Neurosurgery*, Vol. 54 No. 1, pp. 21–28.

Mohamed, O.A., Masood, S.H. and Bhowmik, J.L. (2015), "Optimization of fused deposition modeling process parameters: a review of current research and future prospects", *Advances in Manufacturing*, Vol. 3 No. 1, pp. 42–53.

Nicharat, A., Shirole, A., Foster, E.J. and Weder, C. (2017), "Thermally activated shape memory behavior of melt-mixed polyurethane/cellulose nanocrystal composites", *Journal of Applied Polymer Science*, Vol. 134 No. 27, pp. 1–10.

Özgür Seydibeyoğlu, M. and Oksman, K. (2008), "Novel nanocomposites based on polyurethane and micro fibrillated cellulose", *Composites Science and Technology*, Vol. 68 No. 3–4, pp. 908–914.

Szcześniak, L., Rachocki, A. and Tritt-Goc, J. (2008), "Glass transition temperature and thermal decomposition of cellulose powder", *Cellulose*, Vol. 15 No. 3, pp. 445–451.

Villacres, J., Nobes, D. and Ayranci, C. (2018), "Additive manufacturing of shape memory polymers: effects of print orientation and infill percentage on mechanical properties", *Rapid Prototyping Journal*, Vol. 24 No. 4, pp. 744–751.

Wache, H.M., Tartakowska, D.J., Hentrich, A. and Wagner, M.H. (2003), "Development of a polymer stent with shape memory effect as a drug delivery system", *Journal of Materials Science: Materials in Medicine*, Vol. 14 No. 2, pp. 109–112.

Wen, P., Voshage, M., Jauer, L., Chen, Y., Qin, Y., Poprawe, R. and Schleifenbaum, J.H. (2018), "Laser additive manufacturing of Zn metal parts for biodegradable applications: Processing, formation quality and mechanical properties", *Materials and Design*, Vol. 155, pp. 36–45.

Wu, X., Wagner, R., Raman, A., Moon, R. and Martini, A. (2010), "Elastic deformation mechanics

of cellulose nanocrystals", *TMS Annual Meeting*, Vol. 2, pp. 689–696.

Zhao, W., Liu, L., Zhang, F., Leng, J. and Liu, Y. (2019), "Shape memory polymers and their composites in biomedical applications", *Materials Science and Engineering C*, Vol. 97, pp. 864–883.